Solar water heating system and photovoltaic floating cover to reduce evaporation: Experimental results and modeling

M. E. Taboada[a,*], L. Cáceres[a], T. Graber[a], H. Galleguillos[a], L.F. Cabeza[b] and R. Rojas[c]

[a] Department of Chemical Engineering and Mineral Processing, Universidad de Antofagasta, Campus Coloso, Av. Universidad de Antofagasta 02800, Antofagasta, Chile

[b] GREA Innovació Concurrent, Universitat de Lleida, Edifici CREA, Pere de Cabrera s/n, 25001 Lleida, Spain

[c] Departamento de Ingeniería Química, Universidad Católica del Norte, Avenida Angamos 0610, Antofagasta, Chile

[*]Corresponding author at: Department of Chemical Engineering and Mineral Processing, Universidad de Antofagasta, Av. Universidad de Antofagasta 02800, Antofagasta, Chile

E-mail address: mariaelisa.tabaoda@uantof.cl. Tel: 56 55 2637345

Abstract

The arid conditions in northern Chile restrict the access to water and energy and the development for small mining entrepreneurs. For this purpose, this work describes the experimental behavior of a novel sustainable solar water heating system that is suitable for open ponds combined with floating covers and photovoltaic cells which supply the required energy for water pumping and measurement accessories. The heating is provided through solar panels and coil heat exchanger; the cover has on top photovoltaic cells intended to reduce water loss by evaporation and provide electricity for fluid transport and illumination. For comparison purposes two similar ponds were used for holding water, one heated and the other unheated. The heated pond featured a coil containing an enclosed circulating fluid heated by solar heat collectors. To minimize water evaporation the exposed surfaces of the two ponds were covered by floating elements made of high-density polyethylene with photovoltaic cells on top to supply energy for water pumping and to power auxiliary devices of the system. Predicted daily average water temperature values determined from a heat and mass transfer model using experimental meteorological data over eight months of continuous operation were in very good agreement with measured data. The model developed can be applied to improve the design of real-scale plants.

From the experimental results it was found that in the pond with floating covers water evaporation reduction was greater than 90 % with respect to an uncovered pond. Also the photovoltaic cells placed on the floating cover generated up to 68 Wp /m^2 equivalent to electric power. The global average for the daily water solar heating that was measured in the pond was equivalent to 420 kWH/m^2; this energy can be considered as cost savings in relation to the conventional use of diesel oil. A consumption level for a particular industrial application in small communities will determine the required solar panel surface area.

Keywords: solar energy, modeling, heat transfer, monitoring system.

Nomenclature

A	Area (m^2)	W	Width (m)
Cp	Heat capacity (J $kg^{-1}K^{-1}$)	γ	Psychometric constant (kPa $°C^{-1}$)
E	Water evaporation rate (mm d^{-1})	Δ_s	Slope of the temperature saturation water vapour curve (kPa $°C^{-1}$)
e	Pond wall thickness (m)	η	Heat capture efficiency (dimensionless)
Gr	Grashof number	λ	Heat of Vaporization (J kg^{-1})
H	Height (m)	μ	Viscosity (Pa s)
h	Heat transfer coefficient ($Wm^{-2}K^{-1}$)	ρ	Density (kg m^{-3})
I	Solar radiation flux (Wm^{-2})		
k	Thermal conductivity ($Wm^{-1}K^{-1}$)		
L	Length (m)	Subscripts	
L_{cc}	Characteristic length of the exposed surface (m)	a	Air
		b	Bottom
L_{cb}	Characteristic length of the bottom pond (m)	$coil$	Coil
		$conv$	Convection
L_{cf}	Characteristic length of the floating module (m)	unc	Uncovered pond
		eff	Effective
l_f	Internal height of the floating module (m)	ev	Evaporation
		f	Floating element
m	Water flow through the coil (kg s^{-1})	g	Fiberglass
N	Change in heat storage in the water body ($MJm^{-2}d^{-1}$)	i	Insulation
		ir	Radiation
P_{atm}	Atmospheric pressure (mm Hg)	j	Position of the wall
P_s	Vapor pressure of water (mm Hg)	l	Liquid
P_{pa}	Partial pressure of water ambient (mm Hg)	p	Pond
		po	High density polyethylene

Pr	Prandtl number (dimensionless)	t	Top
Q	Heat flow (W)	w	Wall
Q^*	Net radiation (MJ m^{-2} d^{-1})		
q	Heat flux (Wm^{-2})	Superscripts	
Re	Reynolds number	in	Inlet
RH	Relative humidity (dimensionless)	out	Outlet
ra	aerodynamic resistance (s m^{-1})	int	Internal
T	Temperature (°C)	ext	External
U	Overall heat transfer coefficient ($Wm^{-2}K^{-1}$)		

1. Introduction

Northern Chile, and in particular the Atacama Desert, is one of the most active mining regions in the world, with high levels of production of copper, iodine and several inorganic salts (lithium, potassium, nitrates and others). The area is subject to high levels of global radiation, reaching 2500 kWh/m^2 [1], scarce water resources and nearly complete dependence on external sources for conventional energy inputs such as oil, coal and natural gas. In the context of this energy restriction, there is the alternative of solar energy in an area where the continuity and intensity of solar radiation are among the highest in the world. At the same time, any open water storage is subjected to high water evaporation losses and given the scarcity of water it is necessary to reduce water loss by evaporation. This work addresses both issues.

In this context, regional mining companies recognize the importance of incorporating technologies aimed at more efficient use of water resources and the use of solar radiation as an energy source for their productive processes [2]. Among the services that can be supported with solar energy are lighting, transportation of low to medium weight loads, powering electrical and electromechanical equipment with low to medium energy requirements, heating solutions and the supply of pure water.

In copper mining in particular there is a significant potential for using solar energy to heat solutions in electro-winning and for washing copper cathodes [3]. In order to improve the leaching efficiency of sulfide minerals, a high temperature is required to improve the mineral process like leaching because the extraction increases with the temperature [4]. Generally these processes use fossil fuels that transfer heat to solutions or water through direct combustion at a high economic and environmental cost.

This work investigates the efficiency of a solar water heating system that uses an intermediate heat-carrier fluid flowing in a closed circuit between a solar panel and a water pond considering minimal water loss by evaporation and photovoltaic energy generation as complementing criteria to achieve sustainability and cost effective operation. Thus, the specific attributes of this innovative proposal are that, a) the complementary energy to power auxiliary equipment for the water heating system, such as measuring devices, illumination and recirculating pumps, is provided with photovoltaic energy and, b) the system is provided with a technique for water evaporation mitigation based on the use of high-density polyethylene floating covers.

Studies to mitigate water evaporation have investigated the use of different floating objects, the results of which have been reported in the literature [5-7]. Some of these results indicate that the use of these units allow achieving an evaporation efficiency of over 60% [7].

Under local conditions of aridity, cheap land cost and remoteness from urban centers, the use of solar photovoltaic panels systems and HPDE floating modules is an economically and technologically feasible alternative to be used as a complementary accessory for solar water heater panels in mineral processing plants at Northern Chile. It is interesting to note that floating modules are also very convenient for operation under prevalent local condition of high wind gusts, in addition to pond level variability that occurs during continuous operation.

Recently a combination of floating covers and photovoltaic panels were used in a solar pilot plant experiments for agricultural use [8]. In this plant the photovoltaic panels were fixed on the free surface of the high-density polyethylene modules floating on a water surface reservoir for agricultural irrigation. Thus in this system the water evaporation reduction through a 7 % cover of the reservoir water surface area with floating modules is combined with a photovoltaic energy generation. In a further work a technical economic analysis was made under full surface area coverage of the pond [9].

Other works involving floating photovoltaic panels have been reported in the literature. However the research attention is focused on a restrictive situation of land availability. The results indicate a higher efficiency for these panels in comparison with those installed on land surface. [10-12].

There are studies in the literature of systems for storing solar energy in fluids, the majority considering the use of solar ponds. Earlier works [13-15] studied steady-state solar ponds with

the objective of modeling the stratification of temperature as a function of the depth of the pond. More recent studies [16-22] have been oriented to the dynamic evaluation of this type of system. In general, these works have correctly predicted the temperature profiles in different thermal zones of solar ponds and have found good fits to experimental measurements.

In consideration to the limited information available about systems analogous to that proposed in this work, the experimental pilot plant study was aimed to evaluate the behavior of solar water heating system for mining applications at small and medium scale under imposed conditions of water evaporation reduction and photovoltaic generation. These conditions are compatible with the local situation of a severe shortage of water and a high availability of solar energy. The evaluation was made in reference to a steady state model on daily basis. Bibliographical heat and mass transfer correlations for internal and external liquid-solid and solid-air boundaries were carefully selected and applied to run in a proper numerical program. This analysis will allow a behavior examination of the system in the context of possible modifications in the design and/or conditions of operations, without the need for experimental studies that in general require long periods of time for correct assessment.

2. Experimental part

2.1. Design of the solar energy system and floating elements

The proposed energy storage system was installed on the campus of the Universidad de Antofagasta, Chile (latitude 23°42'5"S/longitude 70°25'8"W). The system is composed of two water storage ponds that operate independently of each other. One of them without heating is used as a blank, that is, a reference to be compared with the behavior of the heated ponds. Both ponds are rectangular and have the same dimensions: 2.51 m long (L_p), and 1.12 m wide (W_p), with a water depth in both ponds of 0.40 m (H_p). Fig. 1 shows the dimensions of the ponds in detail.

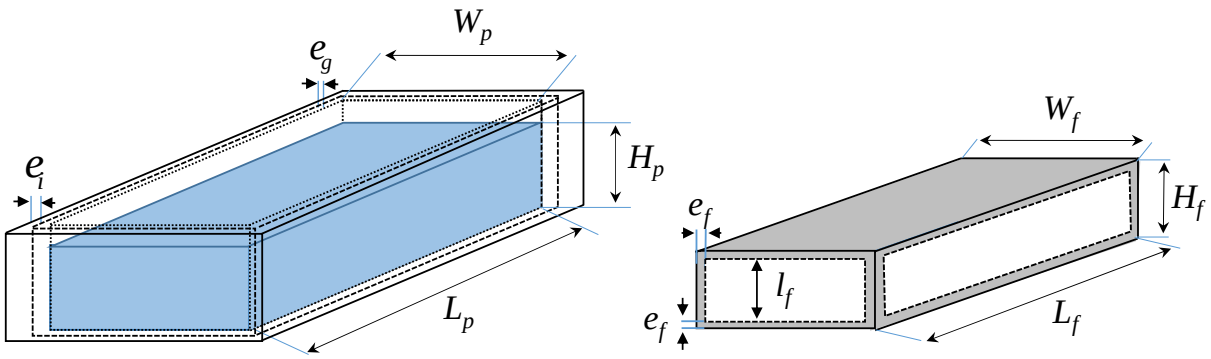

Fig. 1. External and internal dimensions of the ponds and the floating elements

The ponds are made of fiberglass and have a layer of polyester Fiber-Block 330 insulation. The pond walls are 0.005 m thick (e_g) and the insulation layer is 0.11 m thick (e_i) (Fig. 1). The ponds are supported by a metal structure that maintains them 0.6 m above the ground.

With the objective of reducing water loss by evaporation floating objects were placed on the surface of the water in both ponds. Each floating object covers approximately 95% of the cross-sectional area of the pond and is made of high-density polyethylene. The floating elements used in this study were prism-shaped rectangles with the following dimensions: 2.47 m long (L_f), 1.08 m wide (W_f) and 0.1 m high (H_f) (Fig. 1).

The floating objects are 5 mm thick (e_f), with hollow air-filled interiors that ensure buoyancy. This section is 0.09 m high (l_f) (Fig. 1).

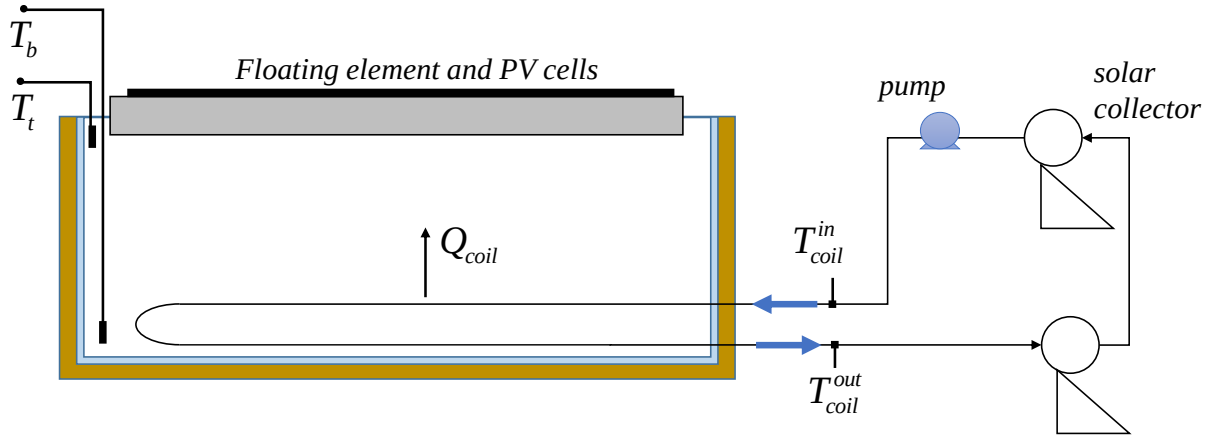

Fig. 2. Pond with solar heating system

The ponds are distinct from each other in that only one has an external heating system that consists of a coil inside the pond and two solar collectors. The coil contains a heat-carrier fluid (distilled water) that allows transporting solar energy absorbed by the collectors to the fluid stored in the pond. The coil is made of annealed copper fixed in the pond bottom. It is 9 m long and has an internal diameter of 8 mm. Figure 2 shows the final configuration for the pond with the heating system.

The HTF is pumped through the coil at constant rate of 25 L/h by an electromagnetic pump (Tekna Evo, model 803 AKS) connected to the solar power supply system.

The ponds have a system for measuring evaporation developed and patented by the authors [23]. The system measures evaporation by determining pond level change in the pond and an automatic repositioning of the evaporated water.

The solar collectors (Stärke) have 15 vacuum tubes connected to an 100 L stainless steel tank. (15 tubes of 5.8 cm diameter x 1 m length)

As well, the solar supply systems are two flexible photovoltaic panels (SOLOPOWER SP1-95) (Table 1), situated on the surface of the floating objects that generate electric energy which is stored in four batteries.

Table 1
Specifications of photovoltaic modules

Electrical Ratings	Value
Maximum Power	95 W
Max. Power Voltage	26.2 V
Max. Power Current	3.60 A
Open Circuit Voltage	34.8 V
Short Circuit Current	4.20 A
Max. Series Fuse	**7** A

The ponds, structural parts including piping and coil tubing were constructed using low cost and easily accessible materials with the aim of having a practical and simple application for implementation in remote mining facilities and/or rural communities.

2.2. Meteorological station

Meteorological data was measured at a HOBO U30 Data Logger weather station (located close to the experimental area). It has four sensors to measure ambient temperature, relative humidity, atmospheric pressure, wind velocity and direction, and solar radiation.

For the temperature and relativity humidity measurement a Temperature/RH smart sensor was used whose specifications state a measurement range between -40°C to 70°C and 0 to 100% with an accuracy of ±0.21°C y de ±2.5% respectively. This device is encased in a sealed compartment that is partially exposed to the ambient air to minimize the influence of direct and diffuse solar radiation and ambient dust. The pressure sensor is a Barometric Pressure smart sensor with range and accuracy specifications of 660 to 1070 mbar and ±3 mbar (at 25°C), respectively. The maximum error is ±5 mbar (-40°C to 70°C). The solar radiation sensor is a Silicon Pyranometer smart sensor with a range and accuracy specifications of 0 to 1280 W/m^2 and ±10 W/m^2 respectively. Sensors were set to record data at 30 min interval.

2.3. Measured variables

Temperature sensors were installed in the two ponds to measure temperature at the bottom (T_b) and at the surface (T_t) of the water. Temperature sensors were also installed at the coil intake $\left(T_{coil}^{in}\right)$ and outlet $\left(T_{coil}^{out}\right)$ (Fig. 2). This information was used to study the heating efficiency and energy contribution of the coil in the system. The temperature sensors were connected to a four-channel HOBO data logger that stores all the information generated from the ponds as readings taken every 10 min.

3. Simulation

3.1. Mathematical model

Fig. 3 shows a mass and energy balance scheme applied to the heated pond with different parameters based on behavior models reported in the current literature for solar ponds.

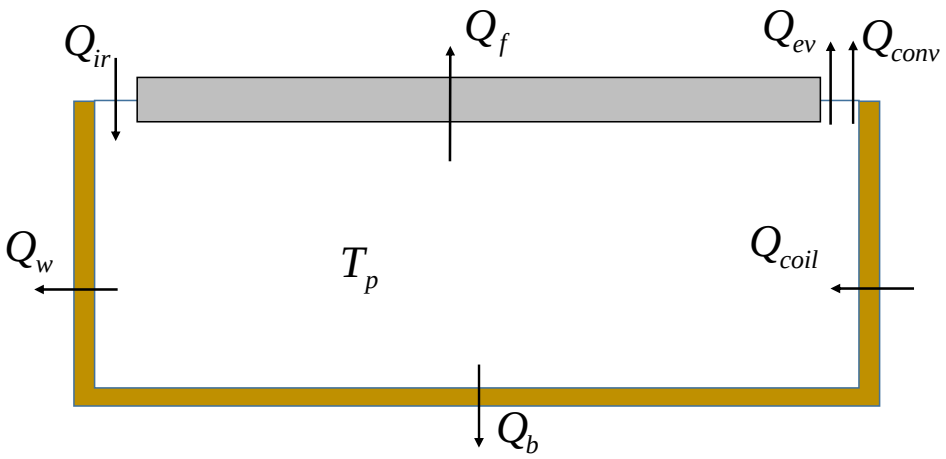

Fig. 3. Heat balance scheme of the water storage pond with external heating. $Q_{coil} = 0$ for water storage pond without external heating.

T_p is the average value from the bottom and surface temperature, Q_{ir} is the heat flow that enters the system by solar radiation, Q_{ev} is the heat flow that leaves the system by evaporation, Q_{conv} is the heat flow withdrawn by forced air convection, Q_w is the heat lost through the walls of the pond, Q_b is the heat lost through the pond bottom, Q_f is the heat lost through the floating elements.

According to Fig. 4, the energy balance in the stationary state condition is:

$$Q_{ir} = Q_{ev} + Q_{conv} + Q_w + Q_b + Q_f \quad (1)$$

In the case of the heating pond, the coil provides an additional source of energy in the system (see Fig. 3). The global energy balance in the stationary state for the heating system is:

$$Q_{ir} + Q_{coil} = Q_{ev} + Q_{conv} + Q_w + Q_b + Q_f \quad (2)$$

where Q_{coil} is the heat provided to the system through the coil walls.

The mathematical expressions for the terms in the material balance (for the two designs) are defined below.

The solar radiation in northern Chile is the main source of energy for the systems under study. The direct solar energy input to the water pond is [18]:

$$Q_{ir} = I\, A_{ir}\, \eta \tag{3}$$

where I is mean solar radiation, A_{ir} is the cross-sectional area of the pond without cover by floating objects, and η is the efficiency in capturing solar energy. The factor η is incorporated to give account for the real quantity of solar energy captured by the water stored in the pond.

Because of a condition of stagnant air of the uncovered surface between the floating elements and the ponds wall, it is assumed that the heat loss mechanism across this water surface is by natural convection. The heat flow that leaves the system by convection is represented by the following expression:

$$Q_{conv} = h_{conv}\, A_{ir} \left(T_p - T_a\right) \tag{4}$$

where h_{conv} is the convective heat transfer coefficient y T_a is the air temperature.

To calculate the energy lost by convection, it is necessary to estimate the convective heat transfer coefficient. For the external horizontal facing up surface in contact with the ambient air, the convective heat transfer coefficient is calculated by the following expression [24, 25]:

$$h_{conv} = 0.15\left(\frac{k_a}{L_{cc}}\right)(Pr\, Gr)^{1/3} \tag{5}$$

where Pr is the Prandtl number, Gr is the Grashof number, k_a is the thermal conductivity of the air and L_{cc} is the characteristic length calculated as the ratio between the area and perimeter of the exposed surface.

In storage water systems a thermal energy is thermodynamically associated to water evaporation from the water surface to ambient air. The heat flow leaving the water surface is proportional to

both, the convective heat transfer coefficient and the water partial pressure difference between the water surface and the ambient air [20, 26-28].

$$Q_{ev} = \frac{\lambda h_{conv}\left(P_s - P_{pa}\right) A_{ir}}{1.6 Cp_a P_{atm}} \tag{6}$$

where λ is the latent evaporation heat of water, P_s is the water vapor pressure at the water surface, P_{pa} is the water partial pressure at the ambient air, P_{atm} is the atmospheric pressure and Cp_a is the specific heat capacity of the air.

The surface water vapor pressure is determined from the Antoine equation [26]:

$$P_s = \exp\left(18.403 - \frac{3885}{T_p + 230}\right) \tag{7}$$

The ambient water partial pressure is determined from relativity humidity [26]:

$$P_{pa} = \left(RH\right)\exp\left(18.403 - \frac{3885}{T_a + 230}\right) \tag{8}$$

where *RH* is the mean daily relative humidity of ambient air.

For comparison purposes the water evaporation losses from uncovered water reservoirs was also computed using Penman-Monteith model. The range of daily water evaporation rates calculated at measured daily average water temperature was between 2 and 7 mm/day (Fig. 10).

Some researchers presented diverse models to estimate the quantity of water lost during evaporation [29-32]. Monteith's evaporation model, known as the Penman-Monteith model, has been used successfully to estimate water evaporation rates from open surfaces and in studies of water losses by evaporation and/or evapotranspiration from crops [33, 34]. A detailed algorithm for calculating the Penman-Monteith model, which was used as guide for the calculations made in this work. Eq. (9) shows the Penman-Monteith model in condensed form [35].

$$E_{unc} = \frac{1}{\lambda}\left(\frac{\Delta_s\left(Q^* - N\right) + 86400\rho_a Cp_a\left(p_v^* - p_{va}\right)/ra}{\Delta_s + \gamma}\right) \quad (9)$$

where E_{unc} is the quantity of water evaporated from a pond exposed to the environment, λ is the heat of vaporized water (MJ/kg), Q^* is net radiation, N *is* the change in stored heat, Δ_s is the slope of the water saturation curve, Cp_a is the heat capacity of the air (MJ/kg K), p_v^* is vapor saturation pressure at the water temperature, p_{va} is the vapor pressure in the air, ra is the aerodynamic resistance, γ is the psychrometric constant.

The meteorological data and the water temperature required as inputs for the Penman-Monteith equation are average daily values. A detailed explanation of every variable of the Penman-Monteith equation is given in the Appendix A.

The total heat lost from the four vertical walls from each pond to the environment is determined according to:

$$Q_w = \sum_{j=1}^{4} U_{w,j} A_{w,j}\left(T_p - T_a\right) \quad (10)$$

where $A_{w,j}$ is the area of the *j-th* wall and $U_{w,j}$ is the global heat transfer coefficient of the *j-th* wall.

According to Eq. (10), in order to estimate the energy lost from the pond walls it is necessary to calculate the global heat transfer coefficient. According to the geometry (Fig. 2), this coefficient for each of the four walls is determined from the following expression [36]:

$$U_{w,j} = \left(\frac{1}{h_{w,j}^{int}} + \frac{e_g}{k_g} + \frac{e_i}{k_i} + \frac{1}{h_{w,j}^{ext}}\right)^{-1} \quad (11)$$

where $h_{w,j}^{int}$ is the internal convective heat transfer coefficient of the *j-th* wall, k_g is the thermal conductivity of the glass fiber, k_i is the thermal conductivity of the thermal insulation material and $h_{w,\mathrm{j}}^{ext}$ is the external convective heat transfer coefficient of the *j-th* wall.

Assuming that the water in the ponds transfer heat to the walls by natural convection, the internal convective heat transfer coefficient $h_{w,j}^{int}$ is estimated using the expression for vertical walls [24, 37]:

$$h_{w,j}^{int} = \left(\frac{k_l}{H_p}\right)\left[0.825 + \frac{0.0387(Gr\ Pr)^{1/6}}{\left[1+\left(0.492/Pr\right)^{9/16}\right]^{8/27}}\right]^2 \tag{12}$$

where k_l is the thermal conductivity of the water.

In the case of the external walls, it is assumed that the surface of the wall loses heat to the environment by forced convection mechanism. The internal convective heat transfer coefficient $h_{w,j}^{ext}$ is evaluated at the corresponding length [24, 38]:

$$h_{w,\mathrm{j}}^{ext} = 0.037\left(\frac{k_a}{L_j}\right)Re^{4/5}Pr^{1/3} \tag{13}$$

where Re is the Reynolds number calculated with the air velocity v_a.

The heat loss through the pond bottom is represented by the following equation:

$$Q_b = U_b\, A_b \left(T_p - T_a\right) \tag{14}$$

where A_b and U_b are the cross-sectional area and is the global heat transfer coefficient of the pond bottom, respectively.

The global heat transfer coefficient is determined according to the geometry shown in Fig. 2.

$$U_b = \left(\frac{1}{h_b^{int}} + \frac{e_g}{k_g} + \frac{e_i}{k_i} + \frac{1}{h_b^{ext}} \right)^{-1} \quad (15)$$

The convective heat transfer coefficient $\left(h_b^{int}\right)$ for the internal bottom surface in contact with water is calculated as:

$$h_b^{int} = 0.15 \left(\frac{k_l}{L_{cb}} \right) (Pr\,Gr)^{1/3} \quad (16)$$

where the characteristic length $\left(L_{cb}\right)$ for the internal bottom surface is calculated as the ratio between the area and perimeter in contact with water

The external convective heat transfer coefficient $\left(h_b^{ext}\right)$ is calculated using Eq. (13) evaluated using the characteristic length for the internal bottom surface.

If we consider the floating element as a composite wall, the heat loss to the environment can be represented as follows:

$$Q_f = U_f A_f \left(T_p - T_a\right) \quad (17)$$

$$U_f = \left[\frac{1}{h_f^{int}} + 2\frac{e_f}{k_{po}} + \frac{l_f}{k_{eff}} + \frac{1}{h_f^{ext}} \right]^{-1} \quad (18)$$

where A_f is the cross-sectional area of the floating element, h_f^{int} is the internal heat convection transfer coefficient, h_f^{ext} is the external heat convection transfer coefficient, k_{po} is the thermal conductivity of the high-density polyethylene and k_{eff} is the effective air thermal resistance.

The internal heat transfer coefficient h_f^{int} was determined from:

$$h_f^{int} = 0.27\left(\frac{k_l}{L_{cf}}\right)\left(Gr\,Pr\right)^{1/3} \quad (19)$$

where the characteristic length for the floating element (L_{cf}) is calculated as the ratio between the area and perimeter of the floating element.

The external convective heat transfer coefficient $\left(h_f^{ext}\right)$ is calculated using Eq. (13) evaluated using the characteristic length for the floating element.

For the determination of the internal heat flow resistance the heat transfer model through air layers was selected [39, 40]. According to this model the air layer inside the floating element is assumed to behave as a solid with a thermal conductivity termed as effective air thermal resistance (k_{eff}), which is determined according to the following expression [41, 42]:

$$k_{eff} = k_a\left(1 + 1.44\left[1 - \frac{1708}{\left(Gr\,Pr\right)}\right]^* + \left[\left(\frac{Gr\,Pr}{5830}\right)^{1/3} - 1\right]^*\right) \quad (20)$$

where the term in square parenthesis for any parameter θ is defined in the following manner:

$$\left[\theta\right]^* = \left(\left|\theta\right| + \theta\right)/2 \quad (21)$$

The heat transfer through the coil heat exchanger is determined according to:

$$Q_{coil} = m_{coil}\,Cp_l\left(T_{coil}^{in} - T_{coil}^{out}\right) \quad (22)$$

where m_{coil} is the water flow through the coil and Cp_l is the heat capacity of the water.

Introducing heat transfer expressions (Eqs. 3, 4, 6, 10, 14, 17 and 22) in Eqs. (1) and (2), as corresponds, yields the final two global heat transfer balance equations.

The global heat transfer balance equation for the unheated pond is:

$$\left[h A_{ir} + \sum_{j=1}^{4} U_{w,j} A_{w,j} + U_b A_b + U_f A_f \right] \left(T - T_a \right) = I \, A_{ir} \, \eta - \frac{\lambda h_{conv} \left(P_s - P_{pa} \right) A_{ir}}{1.6 \, Cp_a \, P_{atm}} \tag{23}$$

And for the heated pond the equation is:

$$\left[h A_{ir} + \sum_{j=1}^{4} U_{w,j} A_{w,j} + U_b A_b + U_f A_f \right] \left(T - T_a \right) = I \, A_{ir} \, \eta + m_{coil} \, Cp_l \left(T_{coil}^{in} - T_{coil}^{out} \right) - \frac{\lambda h_{conv} \left(P_s - P_{pa} \right) A_{ir}}{1.6 \, Cp_a \, P_{atm}} \tag{24}$$

The mathematical model for each pond is defined by a system of two nonlinear algebraic equations. Each energy balance requires the determination of the water partial pressure at the exposed water surface (Eq. 7). Due to the implicit nature of these equations containing the water temperature value to estimate water evaporation, a successive iteration method must be applied for numerical resolution.

3.2. Statistical analysis

To compare the theoretical and experimental results, the correlation coefficient (r) and root mean square percent deviation (ε) have been evaluated by using the following expression [43]:

$$r = \frac{n\left(\sum X_k \times Y_k\right) - \left(\sum X_k\right)\left(\sum Y_k\right)}{\sqrt{n\sum X_k^2 - \left(\sum X_k\right)^2} \sqrt{n\sum Y_k^2 - \left(\sum Y_k\right)^2}} \tag{25}$$

$$\varepsilon = \sqrt{\frac{\left(\sum \varepsilon_k\right)^2}{n}} \tag{26}$$

$$\varepsilon_k = \left[\frac{X_k - Y_k}{X_k} \right] \times 100 \tag{27}$$

3.3. Numeric resolution of the proposed model

The proposed models for the two ponds allow for determining the mean temperature of the stored water based on measured daily average meteorological values of air temperature, wind velocity, relative humidity and solar radiation over a time span of nine months, and also data on physical and transport properties.

For the correct resolution of the proposed system of equations, it is necessary to put attention on adequately estimating two terms. The first is the term that estimates heat losses by evaporation from a correlation widely used in solar pond models (Eq. 6). The second term estimates the quantity of heat incorporated into the system from solar radiation. Calculating this term requires knowing the mean daily radiation value of the exposed area and a parameter that in this article is termed as solar energy capture efficiency η (Eq. 3). Energy capture efficiency was determined based from a month of experimental data (May 2014) from both ponds as the value that minimizes the quadratic error between predicted and experimental mean temperature of the ponds. The remaining data gathered during this study (from June 2014 to January 2015) was used to validate the model based on the obtained η value.

The first step to resolve the equations set for the heated and unheated systems, as described by Eq. (23) and (7), and (24) and (7) respectively, is to assume a mean internal temperature value for the stored water. With this assumed value and the daily average meteorological data the energy balance is resolved to obtain the mean temperature of the water in the pond. The real mean temperature was compared to the supposed value at the beginning of the calculation procedure. This routine is repeated until the temperature difference between the supposed value and the value obtained by the resolution of the model reach a minimal predetermined value. For the purpose of making the calculation, it is assumed that the temperature difference could not exceed 0.01°C. The calculation codes for the two models are programmed in MATLAB.

4. Results

4.1. Experimental results

Fig. 4 shows the daily oscillation temperature range between the minimum and maximum and the average values measured in the two ponds in the bottom for each pond. From this data it is

observed that the daily temperature oscillation that ranges between 2 and 5ºC is similar for both ponds. This oscillation that is due to heat losses taking place at night time exhibit higher values during the summer season.

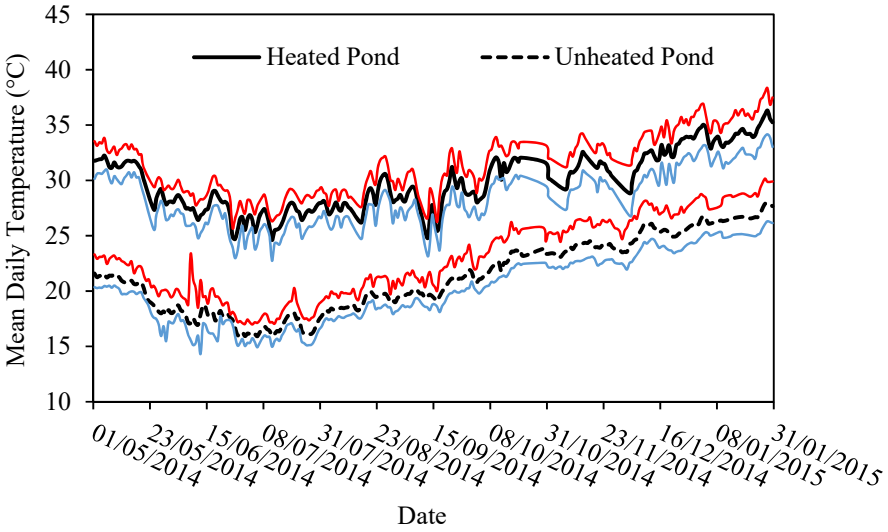

Fig. 4. Comparison of mean (black line), minimum (blue line) and maximum (red line) daily temperatures for the two pond designs

Throughout the study period the difference in mean temperature between the two ponds ranged between 4.6 and 11.7°C, with a mean difference of 8.7°C. The temperature difference between the two ponds decreases slightly as solar radiation increased during the southern hemispheric spring and summer. As shown in Fig. 5, this effect is due to a greater values of the ratio q_{coil} / q_{ir} observed in winter time in comparison to summer time.

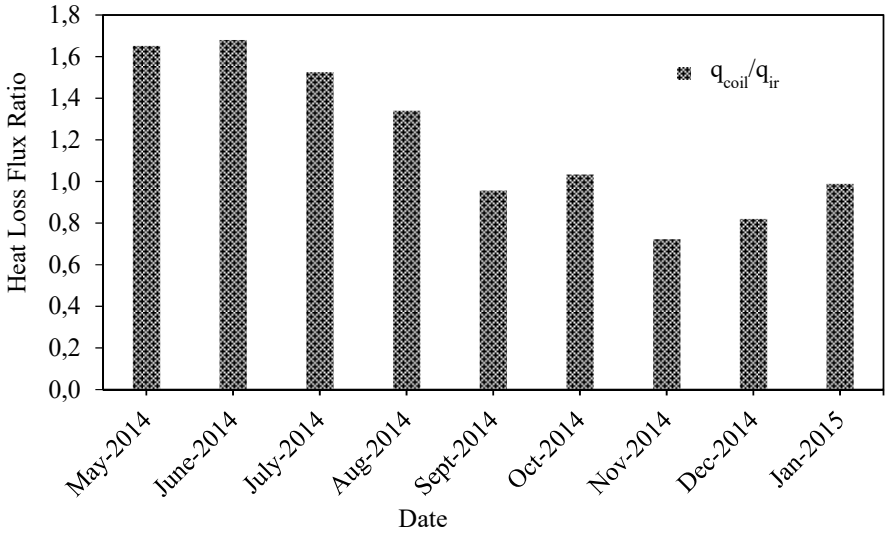

Fig. 5. Monthly variation of mean loss density heat flow ratio

In addition to the internal temperature in the two ponds, the temperature at the inlet and outlet of the coil were also registered. The daily average temperature difference between these two values was 2.4°C. Fig. 6 shows the daily average temperature profiles over the study period.

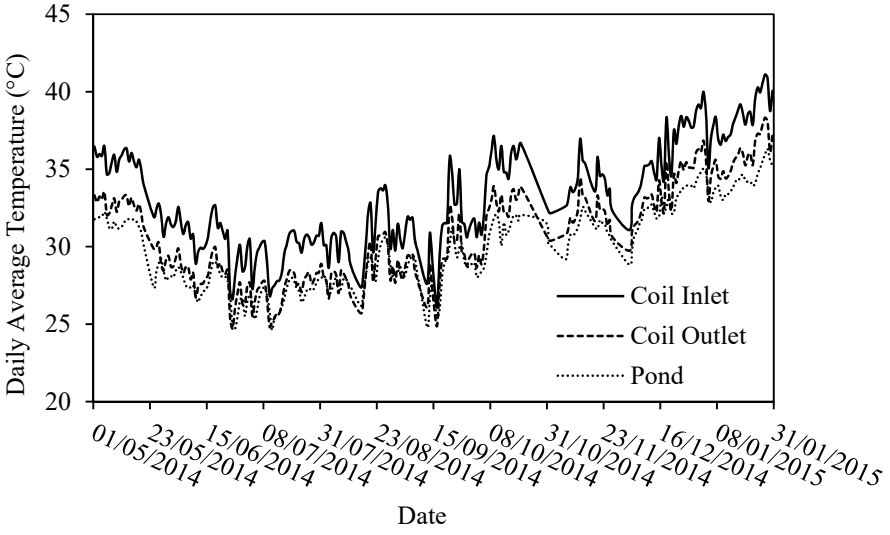

Fig. 6. Thermal behavior of the coil and the heated pond

Table 2 shows the range of variation of the meteorological data gathered during the experimental study and Fig. 7 shows temporal variations along this period. Air humidity and solar radiation

showed the greatest temporal variability. Daily average solar radiation values began to increase in September up to values over 300 W/m^2 in November. Relative humidity ranged between 49.3 and 83.7 % and became more stable as solar radiation increased. Wind velocity and air temperature ranged between 0.8 and 2.7 m/s and 12.9 and 23.1°C, respectively.

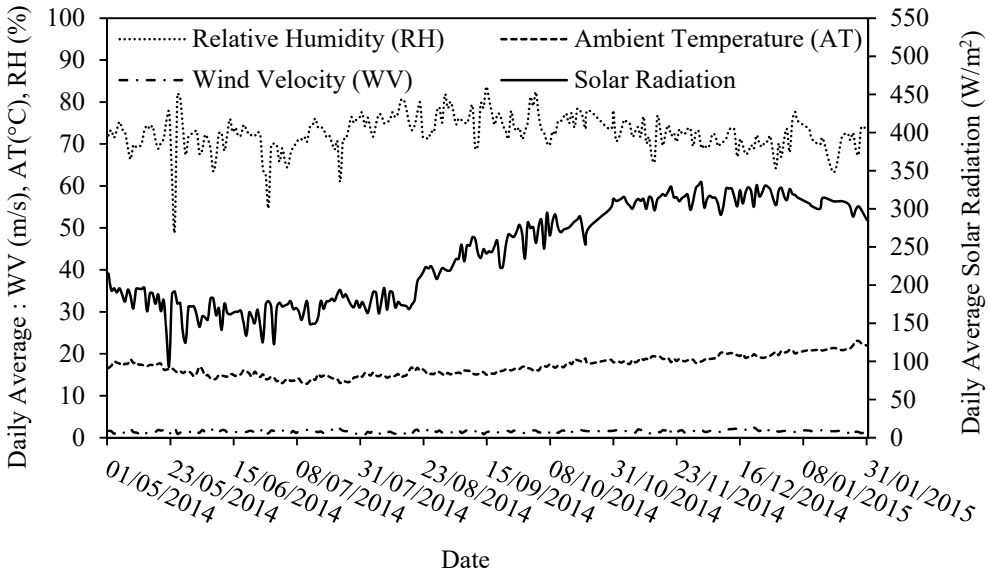

Fig. 7. Meteorological variables during the study

Table 2
Summarize the meteorological variables during the study.

Statistic	Relative Humidity (%)	Solar Radiation (W/m^2)	Ambient Temperature (°C)	Wind Velocity (m/s)
Average	72.7	236.2	16.8	1.5
Standard Deviation	4.2	64.2	2.2	0.3
Minimum	49.3	94.0	12.9	0.8
Maximum	83.7	334.7	23.1	2.7

Although the levels of evaporation between the two ponds do not differ significantly, it can be observed that evaporation rates increases with the level of solar radiation (Fig. 8). The evaporation in covered ponds was reduced to values between 0.1 to 0.4 mm/day in the full study period.

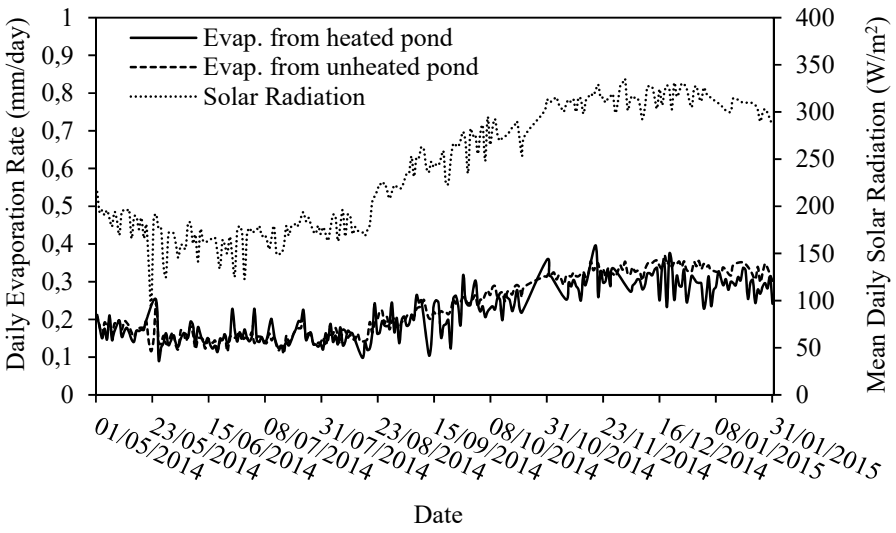

Fig. 8. Water evaporation in the ponds and solar radiation

The Fig. 9 shows the estimated daily average temperature of the floating element external surface of both ponds. No significant differences in these temperatures are observed during all the experimental period. This difference that ranged between 1 and 2 °C should decrease with improved heat insulation efficiency of the materials used for the floating elements. This observation is compatible with the large heat loss observed through the floating element.

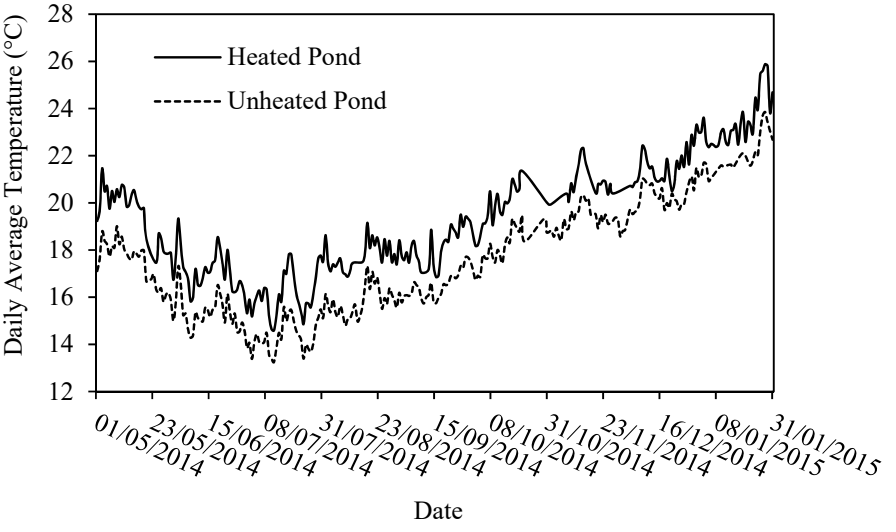

Figure 9. Comparison of daily average temperature of the floating element external surface of both ponds

4.2. Validation of the model

Based on the information gathered over eight months, a period that covered a broad spectrum of solar radiation values, we analyzed the degree of fit of the models proposed in the previous section. The first analysis estimated the efficiency in capturing solar energy. Using the data for the two ponds from May, a mean energy capture efficiency value of 0.85 was calculated. The remaining information was used to validate the proposed models. Fig. 10 shows the level of fit of the model for the unheated pond to the experimental data.

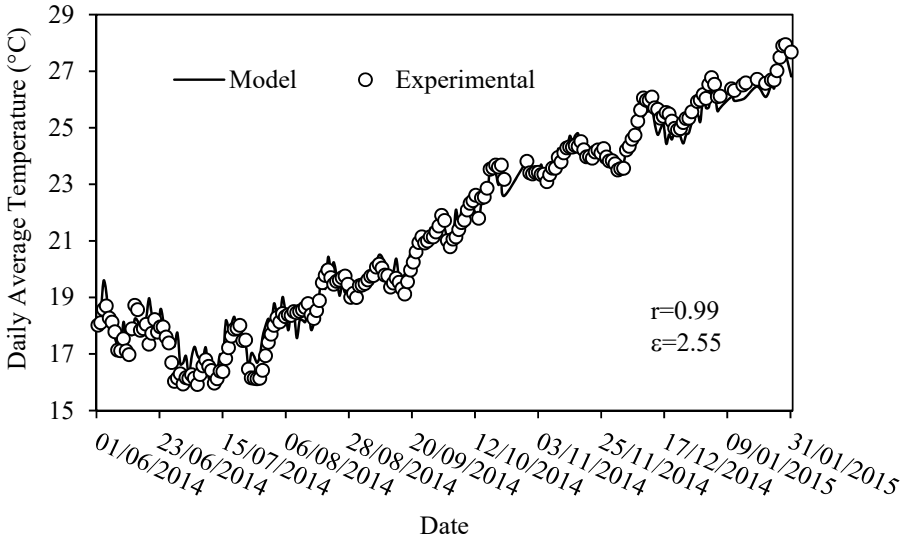

Fig. 10. Comparison of the mean daily temperature modeled for the unheated pond to the mean daily experimental temperature

Fig. 10 indicates that for a value of 0.85 for efficiency in capturing solar radiation, the correlation coefficient and root mean square percent deviation values are 0.99 and 2.55, respectively.

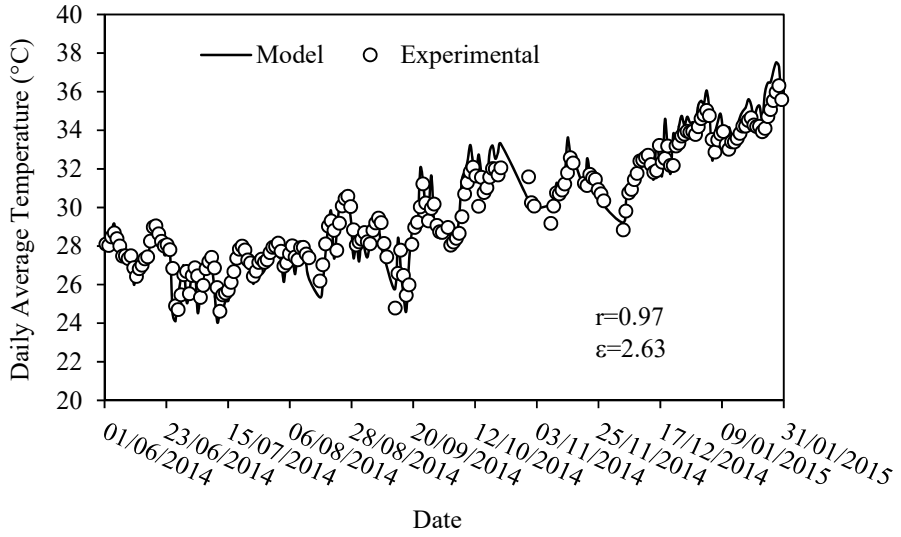

Fig.11. Comparison between the experimental and modeled daily average temperature for the heated pond

Fig. 11 shows the degree of fit of the modeled to the experimental data obtained for the heated pond (for $\eta = 0.85$), which is nearly homogeneously distributed throughout all the experimental period. Despite the slightly larger deviation observed at higher temperatures between modeled and measured values, the chosen procedure to estimate the η value at the lowest temperature season can be considered adequate. This overall degree of fit characterized from the correlation coefficient and the root mean square percent deviation value of 0.97 and 2.63 respectively indicates a good quality of fit.

4.3. Simulation of the water ponds

For energy efficiency assessment a simple simulation model was developed. This model can be use under a wide range of climate conditions and different solutions.

The numerical simulation shows that the effect of covering the exposed area of the unheated pond (approximately 95% of the total area) reduces not only evaporation but also heat loss by mechanism of evaporation and convection. In fact a percentage heat loss value from the total heat losses of 5% was obtained for convection in comparison to 19.6 % for heat losses by evaporation.

505 On average 37.4% of the energy lost is through the floating element, basically owing to the large
506 area exposed to the environment. This indicates that better heat insulation materials should be
507 chosen to improve to the thermal efficiency of the pond (Fig. 12).
508 An aspect of practical interest is the water saving originated from the presence of the floating
509 elements which resulted to be equivalent to 90% of the amount of water evaporation that would
510 be obtained for an uncovered pond. In terms of the average water cost on Northern Chile of 1
511 US$/m^3 this saving are equivalent to 1.8 US$/year/m^2 of covered pond.
512

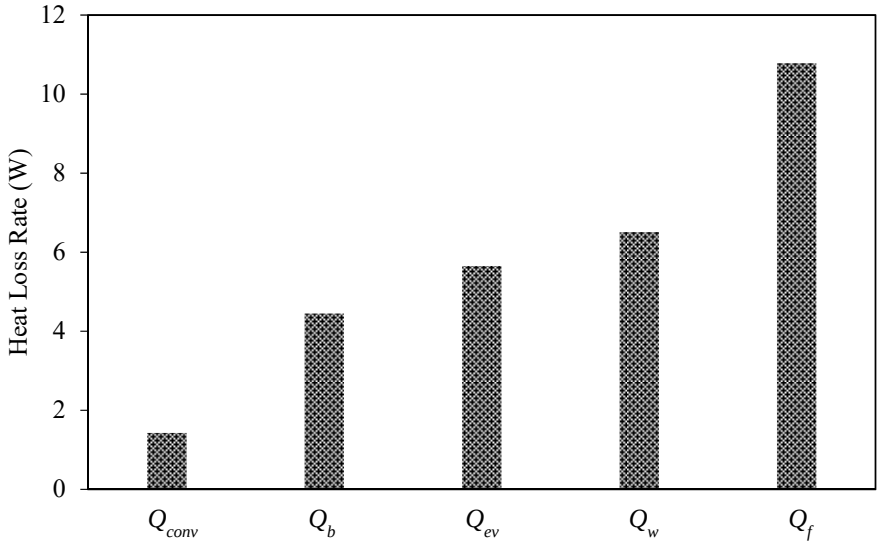

513
514 Fig. 12. Thermal impact of different heat transfer mechanisms in the unheated pond. Each value
515 is the daily average over the experimental time period.
516
517 Fig. 13 indicates that the heat loss by convection, is the factor of highest incidence in the total
518 heat loss of the unheated pond. This is in agreement with the study of solar ponds by Bernard et
519 al. (2013) which indicates that convection and evaporation are the main sources of energy loss
520 for these systems. Owing to the particular design of the two ponds, heat loss by evaporation are
521 significantly reduced in comparison to a pond with a bare water surface (without floating cover),
522 confirming that incorporating the floating elements is a real solution to minimize loss by
523 evaporation.
524
525

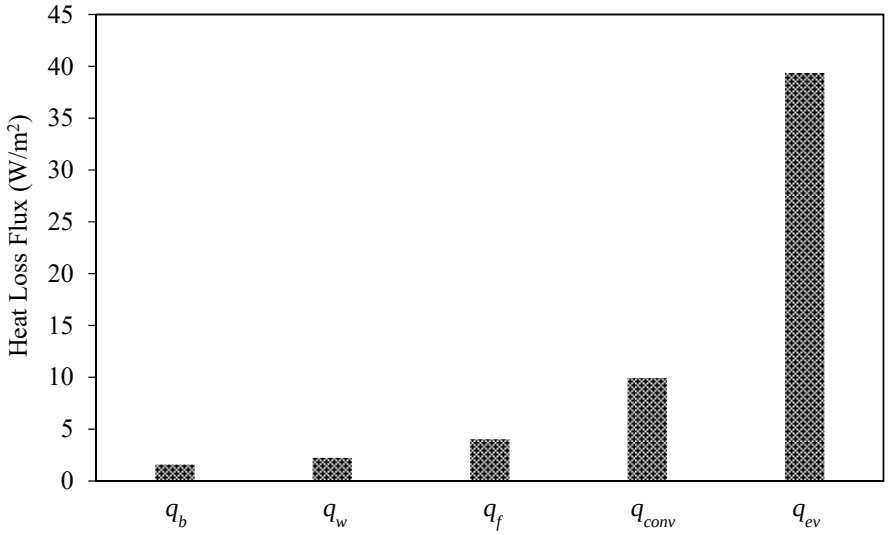

Fig. 13. Thermal impact of the different heat transfer mechanisms in the unheated pond. Each value is the daily average over the experimental time period.

Similar to the observations for the unheated pond, the 95% surface covering of the heated pond resulted in a significant reduction of water evaporation and heat loss. In particular Fig. 14 shows that convection is the least important mechanism responsible for heat loss. In effect, the global incidence of loss by convection and evaporation reaches 6.1% and 20.0 %, of the total heat loss respectively. Again, the major losses to the environment were through the floating element, which reaffirms the need to study the design of this element to maximize the thermal storage capacity of the pond. On average, 40.3 % of the energy lost from the pond to the environment is lost from this section of the pond.

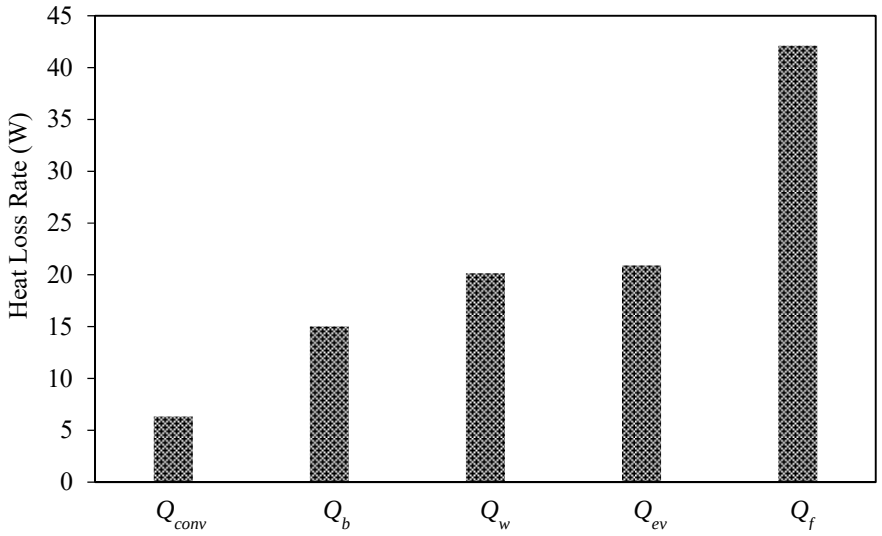

Figure 14. Thermal impact of the different heat transfer mechanisms on the heated pond. Each value is the daily average over the experimental time period.

Using a comparison criterion of density of heat lost flow (Fig. 15), it can be observed that for the case of the unheated pond, the water evaporation is the main source of heat loss.

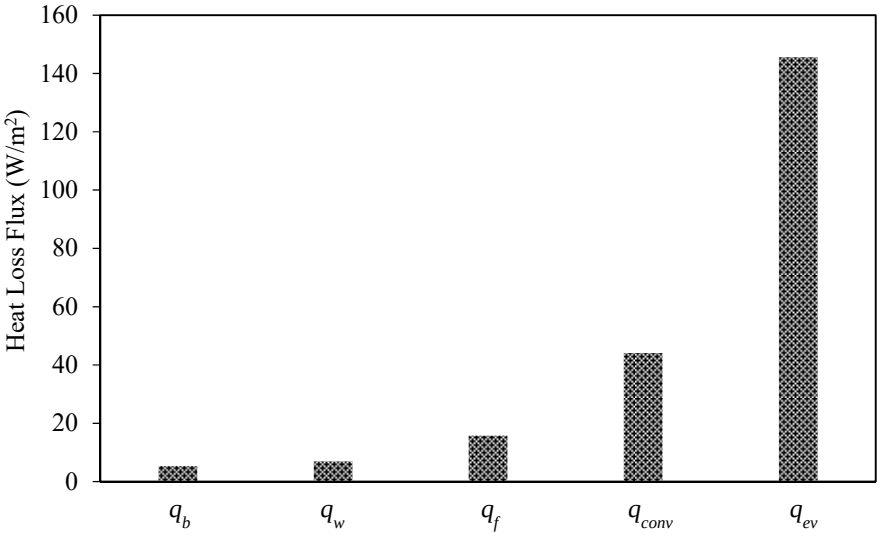

Figure 15. Thermal impact of the different heat transfer mechanisms in the heated pond. Each value is the daily average over the experimental time period.

9. Conclusions

A steady state heat and mass transfer model was developed that is applicable to a pond heated with solar energy, which considers different incoming and outgoing heat flows. The heat flows are determined through meteorological data used in global balances complemented with mass and heat transfer correlations.

The proposed heating system was contrasted and validated by two procedures: 1) comparison to a similar but unheated pond; and 2) comparing the experimental and modeled thermal water profiles. The models for the two systems were validated with experimental data gathered from May 2014 to January 2015. Both models show good fits to the experimental data, reaching correlation coefficients of 0.99 and 0.97. The root mean square percent did not exceed 2.7, which shows a satisfactory fit of the model.

The model simulation shows that both, the heat loss by evaporation and the water evaporation losses, are significantly reduced owing to the presence of the floating elements. This system can also be applied for controlling energy loss in similar units like a water heating system with solar ponds.

The heated pond presents innovative aspects for heat storage and sustainable heating of solutions that is of great interest for leaching and electro winning processes in the copper mining industry. This is because that a moderate increase in process solution temperature would significantly improve the efficiency in metal recovery of these processes.

For application at an industrial scale it is advisable to incorporate a more efficient solar energy collection system than the one employed in this study (domestic thermal collector). It is also advisable to improve the design of the floating elements to increase their thermal resistance and thus minimize heat loss through them.

LUCHO AGREGARA ALGUNAS CONCLUSIONES QUE SACAMOS Y QUE QUEDARON EN ABSTRACT Y OTRAS PARTES DEL TEXTO DESTACADAS PERO FALTA AGREGAR ACA

Acknowledgments.

The authors acknowledge to CONICYT/FONDAP N° 15110019 and Innova Ideas for the financial support. Luisa F. Cabeza would like to thank the Catalan Government for the quality accreditation given to her research group GREA (2014 SGR 123).

581 **Appendix A.**

582 For the water evaporation rate calculation using the Penman-Monteith model (Eq. 9), the
583 following set of equations were used [29].

584

585 • Heat of vaporization λ (MJ kg^{-1}) at ambient temperature:

586 $$\lambda = 2.501 - 2.361\times10^{-3}T_a$$

587

588 • The psychometric constant γ (kPa °C^{-1}) is defined by:

589 $$\gamma = \left(P \cdot Cp_a\right) / \left(0.622\,\lambda\right)$$

590

591 • The aerodynamic resistance *ra* (s m^{-1}) is given by:

592 $$ra = \left(\rho_a\, Cp_a\right) / \left[\gamma\left(f\left(u\right)/86400\right)\right]$$

593 $$f\left(u\right) = \left(5/A\right)^{0.05}\left(3.80 + 1.57v_{10}\right)$$

594 Where *f(u)* (MJ m^{-2} d^{-1} kg^{-1}) is the wind function calculated from the wind velocity (v_{10})
595 measured at 10 m heigth in m s^{-1}, and *A* (km^2) is the tank cross sectional area.

596

597 • The net radiation Q^* (MJ m^{-2} d^{-1}) is calculated from a solar radiation balance between the
598 energy inlet $K\downarrow$ Q^* (MJ m^{-2} d^{-1}) and the incoming and outcoming long wave radiation
599 $L\downarrow$ Q^* (MJ m^{-2} d^{-1}) and $L\uparrow$ Q^* (MJ m^{-2} d^{-1}) respectively.

600 $$Q^* = K\downarrow\left(1-\alpha\right) + L\downarrow - L\uparrow$$

601 $$L\downarrow = \sigma\left(C_f + \left(1 - C_f\right)\left(1 - \left(0.261\exp\left(-7.77\times10^{-4}T_a^2\right)\right)\right)\right)\left(T_a + 273.15\right)^4$$

602 $$L\uparrow = 0.97\sigma\left(T_p + 273.15\right)^4$$

603 Where σ is the Stefan-Boltzmann constant (MJ m^{-2} K^{-4} d^{-1})

604 • The fraction of cloud cover (C_f) is determined according to:

605 If $K_{ratio} > 0.9$ then use $C_f = 2\left(1 - K_{ratio}\right)$

606 If $K_{ratio} \le 0.9$ then use $C_f = 1.1 - K_{ratio}$

607 Ratio of incoming short wave radiation to clear sky short wave radiation (K_{ratio}) is given
608 by:

609 $$K_{ratio} = \frac{K\downarrow}{K_{clear}}$$

610 Clear sky short radiation (K_{clear} en MJ m^{-2} d^{-1}) is calculated by:

611 $$K_{clear} = K_{ET}\left(0.75 + 2\times10^{-5}\psi\right)$$

612 Ψ is the water body altitude in m

613 • Extraterretrial short wave radiation (K_{ET} in MJ m^{-2} d^{-1}) is defined by:

614 $$K_{ET} = \frac{1440}{\pi}\left(0.082 d_r\right)\left(\omega_s \sin(\varphi)\sin(\delta) + \cos(\varphi)\cos(\delta)\sin(\omega_s)\right)$$

615 • Sunset hour angle (ω_s) is determined from:

616 $$\omega_s = \frac{\pi}{2} - \arctan\left(-\tan(\varphi)\tan(\delta)\Big/\left(1-\left(\tan(\varphi)\right)^2\left(\tan(\delta)\right)^2\right)^{0.5}\right)$$

617 • Solar decimation (δ) is calculated using:

618 $$\delta = 0.409\sin\left(\frac{2\pi}{365}J - 1.39\right)$$

619 • The inverse relative distance Earth-sun (d_r) is calculated from:

620 $$d_r = 1 + 0.033\cos\left(\frac{2\pi}{365}J\right)$$

621 J is the day of the year

622 • The wet bulb and dew bulb temperatures (T_n in °C) and (T_d in °C) respectively are:

623 $$T_n = \frac{0.066T_a + \left(4098\,p_{va}\Big/\left(T_d+237.3\right)^2\right)T_d}{0.066 + \left(4098\,p_{va}\Big/\left(T_d+237.3\right)^2\right)T_d}$$

624 $$T_d = \frac{116.9 + 237.3\ln\left(p_{va}\right)}{16.78 - \ln\left(p_{va}\right)}$$

625 where p_{va} is the ambient vapor partial pressure (kPa) determined as:

626 $$p_{va} = (HR)\exp\left(17.27T_a\Big/\left(T_a+237.3\right)\right)$$

627 • The time constant $(\tau \text{ in days})$ is calculated according to:

628 $$\tau = \frac{\rho_l Cp_l Z}{4\sigma\left(T_n + 273.15\right)^3 + f\left(u\right)\left(\Delta_n + \gamma\right)}$$

629 The saturation vapor curve slope (in kPa °C^{-1}) at the wet bulb temperature $\left(\Delta_s\right)$ is
630 determined according to:

631 $$\Delta_n = \frac{4098\left[0.6108\exp\left(17.27T_n/\left(T_n + 237.3\right)\right)\right]}{\left(T_n + 237.3\right)^2}$$

632 • The change in stored heat (N in MJ m^{-2} d^{-1}) in a water tank is calculated from:

633 $$N = \rho_l Cp_l Z\left(T_p - T_{p0}\right)$$

634 where T_{p0} (°C) is the initial water temperature in the tank

635 T_{p0} is a temperature value at the first day of the calculation. For subsequent days this
636 value is the average temperature of the former day.

637 • The saturation vapor curve slope (in kPa °C^{-1}) at the water temperature $\left(\Delta_s\right)$ is calculated
638 from:

639 $$\Delta_s = \frac{4098\, p_v^*}{\left(T_p + 237.3\right)^2}$$

640 • The partial water pressure $\left(p_v^*\right)$ in kPa at ambient temperature is calculated according to:

641 $$p_v^* = 0.6108\exp\left(17.27T_p/\left(T_p + 237.3\right)\right)$$

642

643 **Appendix B.** Efficiency estimation of the solar heating panels.

644

645 Given that the inlet and outlet temperature profiles of the coil are input data for the energy
646 balance, the efficiency of the solar heating panels is estimated here as follows.
647 The heating energy in the coil is:

648 $$Q_{coil} = m_{coil}\, Cp_l\left(T_{coil}^{in} - T_{coil}^{out}\right)$$

649 The solar energy reaching the coil is:

650 $$Q_{collector} = I_r\, A_{collector}$$

651 Where, the exposed surface area for solar radiation was determined as the summation area of the
652 tubes (N_{tubes}) in the solar panels.

653 $$A_{collector} = A_{tube}\, N_{tube}$$

654 Thus,

655 $$\eta_{collector} = \frac{Q_{coil}}{Q_{collector}} \times 100$$

656 Figure, shows the seasonal profile of the solar panel heating efficiency that reaches a maximum
657 value of 20 % following a seasonal tendency by which lower values are seen at colder times.
658 These low values are attributed to the shading conditions of the heating solar panels in the testing
659 place.

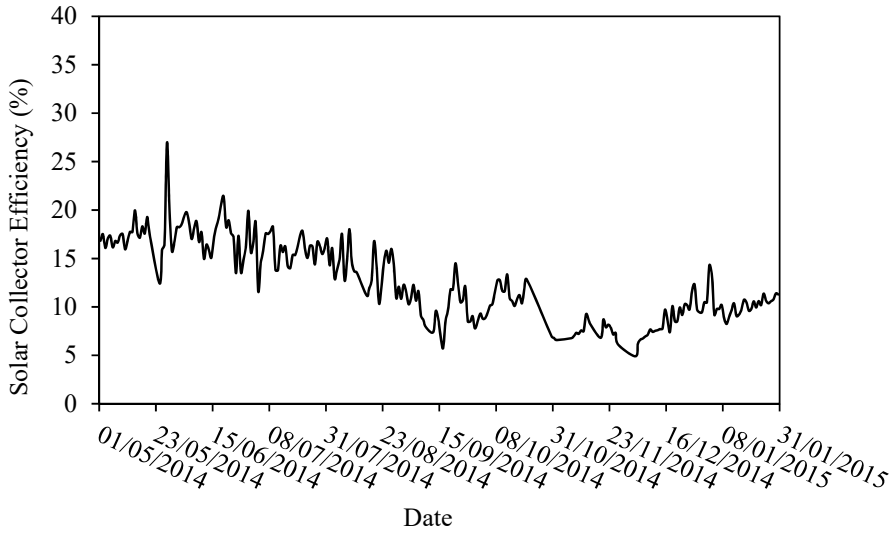

660
661
662
663

664 **References**

665 [1] A.G. Fernández, S. Ushak, H. Galleguillos, F.J. Pérez, Development of a new molten salts
666 with $LiNO_3$ and $Ca(NO_3)_2$ for energy storage in CSP plants, Applied Energy 119 (2014) 131-
667 140.

[2] F. Garrido, R. Soto, J. Vergara, M. Walczak, P. Kanehl, R. Nel, Solar pond technology for large-scale heat processing in a Chilean mine, Journal of Renewable and Sustainable Energy 4 (5) (2012), 053115. http://dx.doi.org/10.1063/1.4757627.

[3] F. Garrido, J. Vergara, Design of solar pond for water preheating used in the copper cathodes washing at a mining operation at Sierra Gorda, Chile, Journal of Renewable and Sustainable Energy 5 (4) (2013), 043103. http://dx.doi.org/10.1063/1.4812652.

[4] C.M. Torres, M.E. Taboada, T.A. Graber, O.O. Herreros, Y. Ghorbani, H.R. Watling, The effect of seawater based media on copper dissolution from low-grade copper ore, Minerals Engineering 71 (2015) 139–145.

[5] I. Craig, A. Green, M. Scobie, E. Schmidt, Controlling Evaporation Loss from Water Storages, Rural Water Use Efficiency Initiative Queensland Department of Natural Resources and Mines, NCEA Publication No 1000580/1 (2005).

[6] P.J. Watts, Scoping study - Reduction of Evaporation from Farm Dams, Final Report to the National Program for Sustainable Irrigation. Feedlot Services Australia Pty Ltd, Toowoomba (2005).

[7] X. Yao, H. Zhang, C. Lemckert, A. Brook, P. Schouten, Evaporation Reduction by Suspended and Floating Covers: Overview, Modelling and Efficiency, Urban Water Security Research Alliance Technical Report No. 28 (2010).

[8] C. Ferrer-Gisbert, J. Ferrán-Gonzálvez, M. Redón-Santafé, P. Ferrer-Gisbert, F. Sánchez-Romero, J. Torregrosa-Soler, A new photovoltaic floating cover system for water reservoirs, Renewable Energy 60 (2013) 63-70.

[9] M. Redón Santafé, J. Torregrosa Soler, F. Sánchez Romero, P. Ferrer Gisbert, J. Ferrán Gonzálvez, C. Ferrer Gisbert, Theoretical and experimental analysis of floating photovoltaic cover for water irrigation reservoirs, Energy 67 (2014) 246-255.

[10] K. Trapani, D. Millar, H. Smith, Novel offshore application of photovoltaics in comparison to conventional marine renewable energy technologies, Renewable Energy 50 (2013) 879-888.

[11] K. Trapani, D. Millar, The thin film flexible floating PV (T3F-PV) array: The concept and development of the prototype, Renewable Energy 71 (2014) 43-50.

[12] Y. Choi, A study on power generation analysis of floating PV system considering environmental impact, International Journal of Software Engineering and Its Applications 8(1) (2014) 75-84.

699 [13] H.M. Ali, Mathematical modelling of salt gradient solar pond performance, Energy
700 Research 10 (1986) 377-384.
701 [14] C.F. Kooi, The steady state salt gradient solar pond, Solar Energy 23 (1979) 37-45.
702 [15] Y.F. Wang, A. Akbarzadeh, A parametric study on solar ponds, Solar Energy 30 (6) (1983)
703 555-562.
704 [16] K.R. Agha, S.M. Abughres, A.M. Ramadan, Design methodology for a salt gradient solar
705 pond coupled with an evaporation pond, Solar Energy 72 (5) (2002) 447-454.
706 [17] I. Ali, S. Madhu, R. Yuvaraj, Thermal modeling of solar pond in matlab, International
707 Journal of Scientific & Engineering Research 3(5) (2012) 988-991.
708 [18] F. Bernard, S. Casas, O. Gibert, A. Akbarzadeh, J.L. Cortina, C. Valderrama, Salinity
709 gradient solar pond: validation and simulation model, Solar Energy 98 (C) (2013) 366-374.
710 [19] M. Berkani, H. Sissaoui, A. Abdelli, M. Kermiche, G. Barker-Read, Comparison of three
711 solar ponds with different salts through bi-dimensional modeling, Solar Energy 116 (2015) 56-
712 68.
713 [20] R. Boudhiaf, M. Baccar, Transient hydrodynamic, heat and mass transfer in a salinity
714 gradient solar pond: A numerical study, Energy Conversion and Management 79 (2014) 568-
715 580.
716 [21] S. Kanan, J. Dewsbury, G. Lane-Serff, A simple heat and mass transfer model for salt
717 gradient solar ponds, International Journal of Mechanical, Aerospace, Industrial and
718 Mechatronics Engineering 8 (1) (2014) 27-33.
719 [22] M. Robitu, C. Inard, M. Musy, D. Groleau, Energy balance study of water ponds and its
720 influence on building energy consumption, Eighth International IBPSA Conference, Netherlands
721 (2003).
722 [23] L.R. Cáceres, P.A. Garrido, M.C. Hernández, O.A. Benavente, Y.O. Zepeda, T.A. Graber,
723 H.R. Galleguillos, M.E. Taboada, Sistema para medición y evaluación automatizada de
724 evaporación en pilas de lixiviación, piscinas o estanques de procesos mineros que comprende un
725 estanque o piscina expuesto a evaporación, un sistema de atenuación de oscilaciones de nivel, un
726 sistema sensor y controlador de nivel, un estanque de agua y un sensor de estado; sistema de
727 evaluación de medidas de mitigación de evaporación. Chilean Patent. Patent No: 2011-002389
728 (2011).

729 [24] F.P. Incropera, D.P. DeWitt, T.L. Bergman, A.S. Lavine, Fundamentals of Heat and Mass
730 Transfer, sixth ed., John Wiley & Sons, USA, 2007.
731 [25] J.D. Kumana, S.P. Kothari, Predict storage-tank heat transfer precisely, Chemical
732 Engineering (1982) 127-132.
733 [26] V.V.N. Kishore, V. Joshi, A practical collector efficiency equation for nonconvecting solar
734 ponds, Solar Energy 33(5) (1984) 391-395.
735 [27] H. Kurt, M. Ozkaymak, A.K. Binark, Experimental and numerical analysis of sodium-
736 carbonate salt gradient solar-pond performance under simulated solar-radiation, Applied Energy
737 83 (2006) 324-342.
738 [28] S. Tundee, P. Terdtoon, P. Sakulchangsatjatai, R. Singh, A. Akbarzadeh, Heat extraction
739 from salinity-gradient solar ponds using heat pipe heat exchangers, Solar Energy 84 (2010)
740 1706-1716.
741 [29] H.A.R. De Bruin, Temperature and energy balance of a water reservoir determined from
742 standard weather data of a land station, Journal of Hydrology 59 (1982) 261-274.
743 [30] J. L. Monteith, Evaporation and the environment. The state and movement of water in living
744 organisms, 19th Symp. Soc. Exp. Biol. (1965) 205-234.
745 [31] H.L. Penman, Natural evaporation from open water, bare soil and grass, Proceedings of the
746 Royal Society A193 (1948) 120-145.
747 [32] C.H.B. Priestley, R.J. Taylor, On the assessment of surface heat flux and evaporation using
748 large scale parameters, Monthly Weather Review 100 (2) (1972) 81-92.
749 [33] R.G. Allen, L.S. Pereira, D. Raes, M. Smith, Crop evapotranspiration - guidelines for
750 computing crop water requirements, FAO Technical Paper 56, Food and Agriculture
751 Organization of the United Nations, Rome (1998).
752 [34] I.P. Craig, R. Mossad, N. Hancock, Development of a CFD based dam evaporation model,
753 11th International Health Summer School, Australia (2006)
754 [35] D.L. McJannet, I.T. Webster, M.P. Stenson, B.S. Sherman, Estimating open water
755 evaporation for the Murray-Darling Basin. A report to the Australian Government from the
756 CSIRO Murray-Darling Basin Sustainable Yields Project (2008)
757 [36] R.B. Bird, W.E. Stewart, E.N. Lightfoot, Transport Phenomena, second ed., John Wiley &
758 Sons Inc., USA, 2002.
759 [37] J.P. Holman, Heat Transfer, tenth ed., Mc Graw-Hill, New York, 2010.

760 [38] J.H. Lienhard IV, J.H. Lienhard V, Heat Transfer Textbook, third ed.,Phlogiston Press
761 Cambridge, Massachusetts, 2002.
762 [39] A. Gallegos-Muñoz, J.A. Balderas-Bernal, C. Violante-Cruz, V.H. Rangel-Hernández, J.M.
763 Belman-Flores, Analysis of the conjugate heat transfer in a multi-layer wall including an air
764 layer, Applied Thermal Engineering 30 (6-7) (2010) 599-604.
765 [40] V. Sambou, B. Lartigue, F. Monchoux, M. Adj, Theoretical and experimental study of heat
766 transfer through a vertical partitioned enclosure: Application to the optimization of the thermal
767 resistance, Applied Thermal Engineering 28 (2008) 488-498.
768 [41] K.G.T. Hollands, T.E. Unny, G.D. Raithby, L. Konicek, Free convective heat transfer across
769 inclined air layers, Journal of Heat Transfer 98 (2) (1976) 189-193.
770 [42] I. Tari, Natural convection simulations and numerical determination of critical tilt angles for
771 a parallel plate channel, Energy Conversion and Management 51 (2010) 685-695.
772 [43] S. Agrawal, A. Tiwari, Experimental validation of glazed hybrid micro-channel solar cell
773 thermal tile, Solar Energy 85 (2011) 3046-3056.